

A catalog of calibrator stars for 200-meter baseline near-infrared stellar interferometry

Antoine Mérand^a, Pascal Bordé^b and Vincent Coudé du Foresto^a

^a LESIA, UMR 8109 Paris Observatory 5, place Jules Janssen, 92295 Meudon CEDEX, (FRANCE)

^b Harvard-Smithsonian Center for Astrophysics, 60 Garden Street, Cambridge, MA 02138, USA

ABSTRACT

We present a catalog of reference stars suitable for calibrate long baseline interferometric observations in the infrared. This work includes and extends the previous catalog by Bordé et al. (2002): in the K band, a precision of 1 % or better can be achieved on the visibility with interferometric baselines up to ~ 200 meters instead of ~ 100 in the preceding version. Angular diameters are computed by way of the absolute spectro-photometric calibration method proposed by Cohen et al. (1999), using IRAS and 2MASS photometric measurements. Our updated catalog contains G8–M0 stars with angular diameters 0.6–1.8 mas (median 1.1 mas) and a median error of 2.1 %. The median magnitudes are 3.5 in K and 6.5 in V. Our grid is dense enough that one would find a calibrator star closer than 10 degrees to any direction on the sky.

1. INTRODUCTION

Long baseline stellar interferometers measure the amount of coherence (i.e. the squared modulus of the coherence factor, sometimes also called the raw visibility amplitude, or raw fringe contrast) between any pair of their subapertures. This quantity needs to be calibrated in order to yield the true visibility of the source, which is the modulus of the Fourier transform of the object's intensity distribution at the spatial frequency B/λ defined by the projected baseline B and the wavelength λ . The squared visibility V^2 of an object is derived from the measure μ^2 of its coherence factor, and from an *interferometric efficiency* factor \mathcal{T}^2 (also called *transfer function*), which accounts for the coherence losses caused by imperfections of the instrument and by the Earth's turbulent atmosphere:

$$V^2 = \frac{\mu^2}{\mathcal{T}^2}. \quad (1)$$

From Eq. 1, it appears that the errors on \mathcal{T}^2 and μ^2 contribute equally to the accuracy of the object squared visibility V^2 . As the interferometric efficiency varies during the night owing to changing instrumental and atmospheric conditions, it has to be frequently sampled, and then interpolated for the time of the science target observation (one can see for example Perrin et al. 1998¹ for details of an interpolation strategy) ensure a reliable calibration. The \mathcal{T}^2 determination is done by observing a reference source (μ_{ref}^2) with a known squared visibility (V_{ref}^2), for which

$$\mathcal{T}^2 \equiv \frac{\mu_{\text{ref}}^2}{V_{\text{ref}}^2}. \quad (2)$$

In practice, observations of the science target are interleaved with observations of reference stars, referred to as *calibrator stars* or *calibrators* for short. The choice of a calibrator is critical as one should be able to predict its intrinsic visibility at the projected baseline of the interferometer, with an accuracy which should be at least

Send correspondance to A. Mérand, E-mail: antoine.merand@obspm.fr. P.B. is a Michelson Postdoctoral Fellow, formerly at LESIA, Observatoire de Paris, now at CfA

as good as the measurement of the raw visibility (more about this in Section 2). For this purpose, Bordé et al. 2002² carefully extracted a catalog of calibrator stars from the spectro-photometric reference stellar network compiled by Cohen et al. 1999,³ hereafter C99. Because of the estimated angular diameter of the selected stars (typically 2.3 mas with an error of 1.2 %), this catalog, hereafter cat. 1, provides calibrators for interferometric baselines up to ~ 100 m in the near infrared. The advent of large interferometers, such as the VLTI and CHARA arrays with maximum baselines of 202 and 330 m, respectively, motivated us to compile a catalog for longer baselines, hereafter cat. 2.

In Sect. 2, we explain why the sensitivity of current interferometers leads us to take as calibrators partly resolved stars instead of point-like sources. Then, we argue that these stars can be safely modeled as uniform disks provided they are carefully selected, and we review two different strategies to make this selection. Last, we explain how to decide if a calibrator is appropriate for a given observation. In Sect. 4, we describe how we built cat. 2 by using³'s method and infrared photometric measurements on stars fainter than in cat. 1. Finally, in Sect. 5, we discuss the main characteristics of cat. 2, in particular we demonstrate the relevance of this new catalog for the VLTI/VISA (the VLT interferometer sub-array, involving the 1.8 m auxiliary telescopes) and the CHARA array.

2. CHOOSING AND MODELING CALIBRATORS

The ideal calibrator is a source for which the intrinsic visibility, using the same observational setup as the science target, can be perfectly predicted. Thus every calibrator needs to be described by a morphological model, so that its true squared visibility can be predicted for the full range of spatial frequencies that can be addressed by the interferometer. As reference sources are chosen among stellar objects, the most common models employed to describe a calibrator are, in increasing number of free parameters:

1. The point source (no free parameters): in that case $V_{\text{ref}}^2 = 1$ at any baseline;
2. The uniform disk (UD model), with the angular UD diameter θ as the only free parameter: the monochromatic squared visibility is then given by the relationship:

$$V_{\text{UD}}^2(x) = 4 \left(\frac{J_1(x\theta)}{x\theta} \right)^2, \quad (3)$$

where J_n denotes the n th Bessel function of the first kind and x the spatial frequency, namely $\pi B/\lambda$ (B , baseline and λ the observing wavelength);

3. The limb darkened disk (LD model), with two or more free parameters.

For simplicity and reliability, more complex calibrator models should be avoided. These include non centrosymmetric or variable morphologies like pulsating or flare stars, fast rotators, and binary stars (depending on the separation, binaries can cause trouble to the one of the servo systems, be it the tip-tilt system or the fringe tracker). Indeed, a good calibrator needs to be:

1. *Well modeled*, in the sense that the model which is used to describe the morphology of the object is as simple as possible, yet appropriate within the level of accuracy required for the visibility;
2. *Well known*: the free parameter(s) in the model need to be known with sufficient accuracy;
3. *Stable*: no time dependency of the morphology;
4. Observable with the same setup and in the same conditions as the science target, e. g. close to the target on the sky, with comparable magnitude and preferably spectral type.

It should be noted that these requirements are conflicting since in general they call for references much smaller than the science targets, yet having approximately the same color and apparent brightness, which is impossible for thermal sources. Therefore the choice of a calibrator will always be the result of a compromise. The first and last requirements exclude the point source model in almost every circumstance for long baselines, as it would imply an unrealistically small (hence faint) reference. For example, in order to induce a bias smaller than 1% ($V^2 > 99\%$), a reference star considered as a point source with a 300 m baseline at $\lambda = 2.2 \mu\text{m}$ needs to have an angular diameter smaller than 0.1 mas. If the source is a K0 giant, this corresponds to an infrared magnitude $K \approx 8$, beyond the sensitivity limit of interferometers with small or medium size telescopes.

It happens that quiet single stars can easily and correctly be modeled as uniform disks, when the squared visibility exceeds $\approx 40\%$, regardless of the center-to-limb darkening, as the difference between a UD and a LD model is then smaller than 0.1%. Stellar angular diameters can be known from direct high-angular resolution measurements (interferometry or Lunar occultations) or estimated indirectly by (spectro-)photometry. We argue that a spectrophotometric estimate of the diameter is more suitable for reference purposes, because direct diameter measurements have only been performed on a limited number of sources (they are listed in the Catalog of High Angular Resolution Measurements, hereafter CHARM (Richichi and Percheron 2002⁴), and most of these sources do not have the properties required for being a good calibrator at long baselines. Besides, the interferometric data set is in essence heterogeneous and, more specifically, UD values are published usually at a single wavelength. Because of limb darkening, they are not readily valid for other band-passes. Therefore, in absence of an exhaustive and homogeneous set of direct diameter measurements of suitable calibrator stars (a certainly much needed, however intensive, observational program), we prefer in the remainder of this paper to apply an indirect method to determine the diameters for a set of stars that are selected so that they can be trusted as single and stable.

3. THE CALIBRATOR DECISION DIAGRAM

The purpose of the calibrator decision diagram described here is to find the right calibrator for a given observation. In order to achieve the desired precision for a given instrumental configuration, calibrators have also to be selected according to their diameters and diameter errors. For the UD model, the stellar angular diameter contains all the knowledge on the source, thus the squared visibility error associated with the calibrator error is

$$\left(\frac{\sigma_{V^2}}{V^2}\right)_\theta = \frac{\partial V^2 / \partial \theta}{V^2} = 2x\theta \frac{J_2(x\theta)}{J_1(x\theta)} \frac{\sigma_\theta}{\theta}. \quad (4)$$

As the knowledge of the calibrator should not be the limiting factor on the precision of the visibility measurement, we require for the calibrator choice that the relative error on the squared visibility, σ_{V^2}/V^2 , due to the uncertainty on the calibrator diameter alone, σ_θ/θ , should not exceed the internal (instrumental) error, σ_{μ^2}/μ^2 , that is to say

$$\left(\frac{\sigma_{V^2}}{V^2}\right)_\theta \leq \left(\frac{\sigma_{\mu^2}}{\mu^2}\right). \quad (5)$$

This inequality can be turned into a *decision diagram* that helps decide whether a calibrator is suitable or not for a given observation. In the framework of the UD model and leaving aside magnitude and spectral type considerations, a given source can be represented as a point in a plane diameter/diameter error, i. e. $(\theta, \sigma_\theta/\theta)$. We refer to this plane as the *calibrator plane*. As for the instrumental configuration, all needed information is embedded in the pair spatial frequency/instrumental precision, i. e. $(x, \sigma_{\mu^2}/\mu^2)$ or alternatively in the triplet wavelength/projected baseline/instrumental precision, i. e. $(\lambda, B, \sigma_{\mu^2}/\mu^2)$. By holding two of these three quantities fixed, one can plot the third one as a function of the diameter and diameter error. We call this plot the *calibrator decision diagram*.

As a first example, we set on Fig. 1 the wavelength to $2.2 \mu\text{m}$, the baseline to 200 m, and we plot contours of the instrumental precision in the calibrator plane. In that case, if one wants σ_{V^2}/V^2 to be at most 2%, the diagram shows that either $\theta \leq 1.3$ mas with a 1% error or $\theta \leq 0.65$ mas with a 5% error is required. It is noteworthy that for $\sigma_{V^2}/V^2 \leq 2\%$ and $\sigma_\theta/\theta \geq 1\%$, the squared visibility stays above 40% (corresponding to a $\theta = 1.3$ mas star, observed at $\lambda = 2.2 \mu\text{m}$, with a 200m baseline), which assures of the validity of the UD model

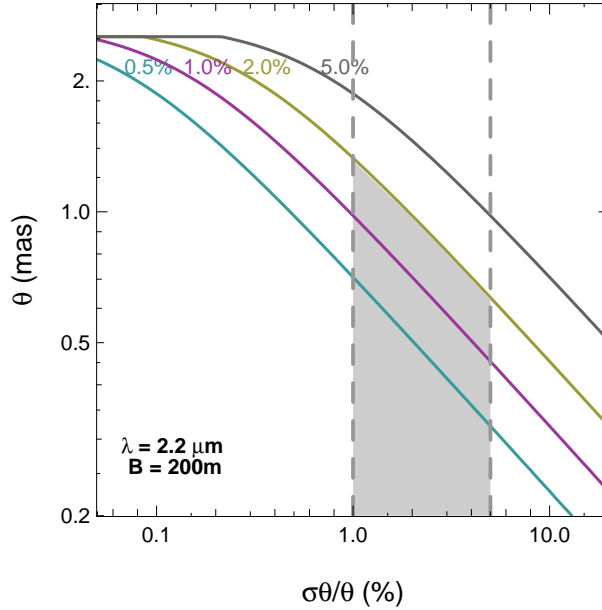


Figure 1. Calibrator decision diagram (logarithmic scales) fixing the wavelength to $2.2 \mu\text{m}$ and the baseline to 200 m : contours of the instrumental precision as a function of the diameter and diameter error of the calibrator. Stars below a given contour could be used at the labeled precision. Vertical dashed lines delimit the area corresponding to the typical diameter error obtained through (spectro-)photometric determinations (1–5 %).

as discussed previously. For this reason, we keep in the following these requirements on the squared visibility and angular diameter precisions.

As a second example, we set in Fig. 2 the wavelength to $2.2 \mu\text{m}$, the instrumental precision to 2 %, and we plot contours of the baseline in the calibrator plane. Open circles represent stars flagged as single and with no shell in CHARM, and open squares represent stars from cat. 1. Stars located below a given contour can be used as calibrators at the corresponding baseline. It appears from this plot that CHARM provides calibrators for projected baselines up to $\sim 70 \text{ m}$, and cat. 1 for baselines up to $\sim 100 \text{ m}$, not being too stringent on the sky coverage.

4. BUILDING THE CATALOG

4.1. How to expand Cat. 1: better models or smaller stars?

Looking at Fig. 2, there are two ways in which cat. 1 could be expanded to satisfy the 2 % precision at 200 m baselines:

1. Decrease the diameter errors by improving the calibrator models (going leftwards on the diagram);
2. Decrease the stellar diameters by finding smaller stars (going downwards on the diagram).

The first solution necessitates working with more resolved stars which necessitates more elaborate models than the UD, along with high-quality observations to determine the parameters of these models. Keeping with our objectives of simplicity and reliability, we favor the second approach, which consists in going only to smaller stars since we guaranty hereby the validity of the UD model. On the other hand, we have to be very careful not to degrade the error. The second solution features the drawback of working with fainter stars. Indeed, the angular diameter logarithmic scale on Fig. 2, can be viewed as a linear magnitude scale for a given spectral type (a given temperature).

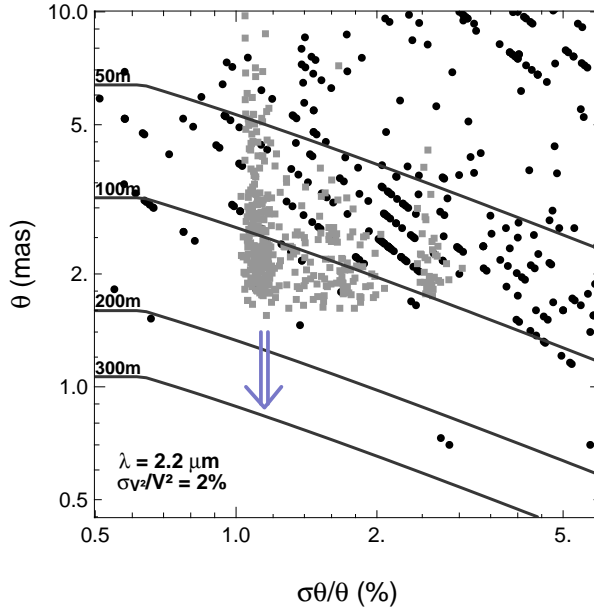


Figure 2. Calibrator decision diagram (logarithmic scales) fixing the wavelength to $2.2\mu\text{m}$ and the instrumental precision to 2 %: contours of the baseline as a function of the diameter and diameter error of the calibrator. Stars below a given contour can be used at the labeled baseline. Stars from cat. 1 appear as gray squares and stars from CHARM as black circles. The double arrow indicates the direction we chose to follow to expand cat. 1. The 50, 100, 200 and 300 m curves in the K band ($\lambda = 2.2\mu\text{m}$) corresponds respectively to 35, 75, 145 and 220 m in the H band ($\lambda = 1.6\mu\text{m}$) and 25, 55, 110 and 165 m in the J band ($\lambda = 1.2\mu\text{m}$).

4.2. Pushing the spectro-photometric method further

Through their whole series of papers Cohen et al. built an all-sky network of absolute reference sources for spectro-photometry in the infrared. The tenth paper,³ exposes at length their method: by fitting low-resolution composite spectra to infrared photometric measurements, they derive both absolute spectral irradiances and stellar angular diameters. Their grid stars were selected from the IRAS Point Source Catalog (hereafter IRAS PSC) by applying stringent quality criteria that qualify most of these stars as interferometric calibrators as well. Cat. 1 was then built by removing the very few stars that would depart from a UD at low resolution.

In their original work,³ used the following 6 criteria in order to select calibrator candidates in the IRAS PSC:

1. The IRAS flux at $25\mu\text{m}$ must be greater than 1 Jy;
2. IRAS infrared colors are restricted to one particular quadrant, corresponding to giant stars;
3. IRAS candidates must be as normal as possible: sources flagged as non-stellar, variable, emission line or carbon stars are rejected;
4. Total IRAS fluxes within a radius of $6'$ must be less than 5 % of the IRAS candidate corresponding fluxes;
5. IRAS stars must not be associated with a small extended source. The contribution of infrared cirrus must be less than 5% of the candidates infrared flux;
6. To reduce the chance of selecting variables, candidates must fall in one of the following spectral and luminosity classes:
 - A0–G9 and II–IV,
 - K0–M0 and III–V.

Walking in the tracks of Cohen et al. 1999,³ we applied the previous set of criteria to the IRAS PSC, modifying criterion 1 to $F_{25\ \mu\text{m}} \leq 1\ \text{Jy}$ in order to sort out new stars. We also required the stars to be identified in the Simbad database to make possible further quality filtering (criteria 3 and 6). A total of 8313 stars passed criteria 1 and 2, as well as the identification by Simbad. In the selection process, we found the 5th criterion – meant to remove stars blended with interstellar cirrus – severely impairs the sky coverage around the Galactic Equator. Therefore, we decided to leave aside that criterion, and to rely instead on the quality of the spectrum fit to the infrared photometric measurements.

4.3. Discarding candidates that depart from a UD

We first removed all known spectroscopic and astrometric binaries using their Simbad object type. However, because of Simbad’s hierarchical classification, a star can have a companion without being classified as a binary. For this reason, we also used the Catalog of Visual and Double Stars in Hipparcos (Dommanget et Nys 2000⁵) to remove all stars with a companion within $2'$. This distance represents a safe upper limits for tip-tilt servo or any other pointing device. Finally, the Hipparcos Catalog (Perryman et al. 1997⁶) was used in order to remove known variables, as well as stars with a positive “Proxy” flag, corresponding to stars with known Hipparcos field stars within $10''$. In order to discard more variable stars or unresolved binaries, we used several catalogs of radial velocity measurements. First of all, Malaroda et al. 2001⁷ collected from the literature all radial velocity measurements into a single catalog. Each entry of this catalog also contains the nature of the object according to each author. If a single author suspected a star to be a spectroscopic binary, this candidate was discarded. Further more, we looked for other measurements which took place after 1998, the upper limit of Malaroda et al. 2001⁷ work: de Medeiros and Mayor 1999⁸ and Nidever et al. 2002⁹ contain more recent material and were used in same manner as we did the Malaroda et al.⁷ Nevertheless, considering the large number of candidate stars, it was out of question to check every one of them in the literature, and to perform dedicated observations where it would have appeared necessary. Therefore, we would like to draw the attention of the reader to the fact that a few stars which are improper for calibration may remain in our published list.

4.4. Photometry

Deriving angular diameters with³s method requires absolute photometric data between 1.2 and $35\ \mu\text{m}$. We used $12\ \mu\text{m}$ and $25\ \mu\text{m}$ photometric data from the IRAS PSC (our input catalog), as well as those from the IRAS FSC (Faint Source Catalog). We extracted the near-infrared photometry, H and Ks magnitudes, from the Two Micron All Sky Survey Point Source Catalog (hereafter 2MASS PSC) absolutely calibrated by Cohen et al. 2003.¹⁰ The 2MASS PSC was the only near-infrared catalog that matches our needs in terms of sky coverage. However, we had to deal with a poor photometric precision ($\sigma_K = 0.25$) for the bright stars ($K = 3-4$) we are interested in, as they tended to saturate 2MASS detectors.

We looked for interstellar extinction by computing the color and comparing it to its expected value for a given spectral class. If A_λ is the extinction in magnitude, the interstellar medium is characterized by $R_V = A_V/(A_B - A_V) = A_V/E_{B-V}$. We used an average of $R_V = 3.1$. Then, thanks to the tables of A_λ/A_V from Cardelli et al. 1989,¹¹ we corrected the H and K magnitudes for reddening. However, this correction always stays within the photometric error bars, because our candidates are bright stars that are close and for which 2MASS photometry is not very accurate. Therefore our relatively crude estimation of the reddening is appropriate.

4.5. Deriving limb-darkened diameters from stellar templates

Stellar templates computed by³ consist in absolute composite spectra for different spectral types and luminosity classes, along with limb-darkened (LD) angular diameters ϕ . Because³ used plane-parallel Kurucz model atmospheres, their LD angular diameters (ϕ) correspond to Rosseland angular diameters, associated with a Rosseland optical depth of unity. Indeed, this diameter corresponds to the zone where photons from the continuum are emitted, and where the center-to-limb variation (CLV) drops to zero. In the case of plane-parallel models, the CLV drops to zero at the stellar limb, i. e. the Rosseland diameter is equal to the limb darkened diameter ϕ (see discussion in Wittkowski et al. 2004¹²).

After retrieving the spectral types and luminosity classes of our candidate calibrators from Simbad, we fitted the absolute template corresponding to a specific star to its infrared photometric measurements. All photometric

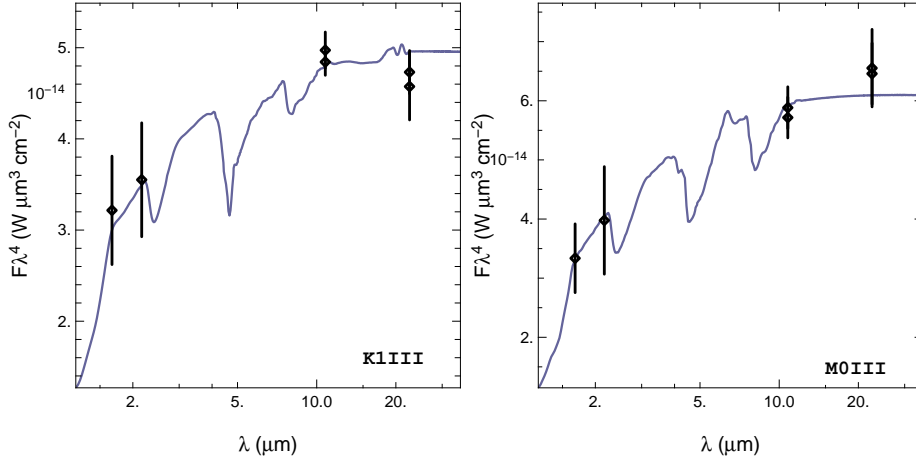


Figure 3. Examples of stellar template fits to photometric measurements converted into monochromatic irradiances at isophotal wavelengths. The data points stand for (from left to right): H, K_s (2MASS), $F_{12\ \mu\text{m}}$ and $F_{25\ \mu\text{m}}$ (IRAS PSC and FSC). *Left:* HD 15248, a K1III star ($\chi_r^2 = 0.39$). *Right:* HD 164724, a M0III star ($\chi_r^2 = 0.22$).

measurements were converted into isophotal quantities, following the calibration prescribed by C99 for IRAS PSC and FSC, and by Cohen et al. 2003¹⁰ for 2MASS PSC. Fig. 3 shows two examples of stellar template fits.

The scaling factor resulting from the fit, l , yielded the LD diameter of the star

$$\phi = \sqrt{l} \times \phi_{\text{ref}}. \quad (6)$$

For every diameter, we computed an associated error by taking into account the contributions of the fitting formal error, σ_l , corresponding to $|\chi^2(l) - \chi^2(l \pm \sigma_l)| = 1$, and of the original template diameter error, $\sigma_{\phi_{\text{ref}}}$, according to

$$\left(\frac{\sigma_\phi}{\phi}\right)^2 = \left(\frac{\sigma_l}{2l}\right)^2 + \left(\frac{\sigma_{\phi_{\text{ref}}}}{\phi_{\text{ref}}}\right)^2. \quad (7)$$

We could not find in³ the angular diameter errors of their original templates. By comparing the diameters published by these authors and the ones computed by our implementation of their method, this internal error was determined to be $\sigma_{\phi_{\text{ref}}}/\phi_{\text{ref}} = 1.03\%$. This value appeared to be unique with respect to spectral type and luminosity class.

As mentioned at the end of Sect. 4.2, we used the quality of the template fit as a filtering tool to ensure the consistency of our method. Namely, if the reduced χ^2 , i. e. $\chi_r^2 = \chi^2/(N - P + 1)$, where N is the number of data points and P the number of parameters, is greater than 1, we exclude the star from the final selection.

4.6. From limb-darkened to uniform disk diameters

We converted LD diameters into UD diameters in J, H and K bands by using the following four-coefficient limb-darkening law from¹³

$$I(\mu) = 1 - \sum_{k=1}^4 a_k (1 - \mu^{k/2}), \quad (8)$$

where I is the specific intensity and μ the cosine of the angle between the line of sight and the perpendicular to the stellar surface.¹³ has tabulated the coefficients a_k according to the stellar effective temperature T_{eff} and surface gravity $\log(g)$.

Only 99 of our candidates could be found in the Cayrel de Strobel et al. 2001¹⁴ catalog of effective temperature and surface gravity measurements, all of them with a spectral type G8–K4. For all others, we estimated T_{eff} by

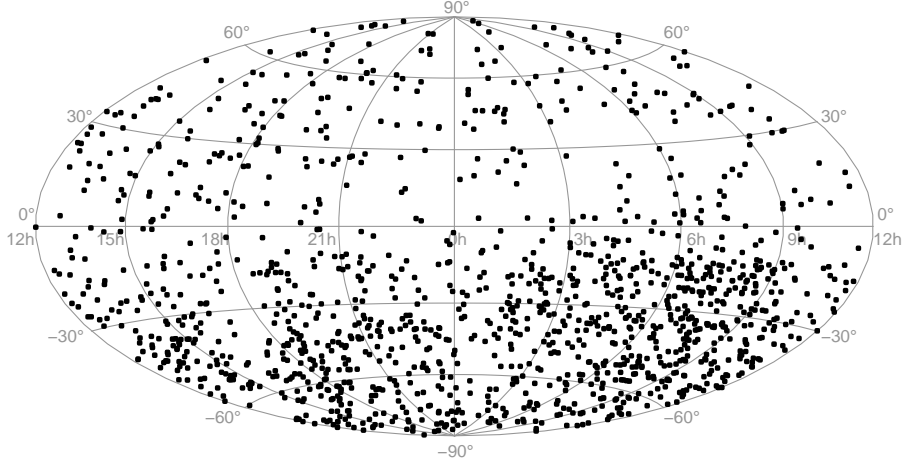


Figure 4. Sky coverage of cat. 2 in equatorial Hammer-Aitoff representation.

Dist. to the closest calib.	Northern Hem.	South. Hem.
less than 3.75°	50 % (15 %)	85 % (30 %)
less than 5°	75 % (25 %)	95 % (40 %)
less than 10°	99 % (55 %)	100 % (65 %)

Table 1. Sky coverage characteristics: area of the sky having corresponding distance to the closest calibrator. Details for northern (positive declination) and southern (negative declination) hemispheres are given. The number in brackets corresponds to a reduced version of Cat. 2, containing only stars that can achieve a 2 % visibility error for baselines greater than 200m in K (which corresponds to 145m in H, 110m in J).

using the Bessell et al. 1998¹⁵ polynomial relation based on the color index $V - K$. When no measurements were available, we used the typical surface gravity for the spectral class, as well as solar abundances. This is legitimate since the infrared limb-darkening is not very sensitive to these parameters.

Taking into account a center-to-limb variation, the visibility function becomes

$$V_{LD}(x) = \frac{\int_0^1 I(\mu) J_0(x \phi \sqrt{1 - \mu^2}) \mu d\mu}{\int_0^1 I(\mu) \mu d\mu}. \quad (9)$$

UD diameters in J, H and K, were obtained by fitting V_{UD} (Eq. 3) to V_{LD} (Eq. 9) in the domain of validity of the UD model, i. e. $V^2 \geq 0.4$. In this domain, the relative difference between the two visibility profiles is less than 10^{-3} .

5. MAJOR CHARACTERISTICS OF THE CATALOG

5.1. Sky coverage

Cat. 2 overall sky coverage is such that there is always a calibrator closer than 10° whatever the location on the sky (Table 1). Moreover, if we keep only stars that can achieve a 2 % visibility error for baseline greater than 200m in K (145m in H, 110m in J), the calibration appears to be still feasible for more than half the sky. The northern hemisphere happens to be less populated than the southern one (Fig. 4), because more stars were filtered out in this part of the sky due to an unsatisfactory spectral type identification with Simbad. For the southern hemisphere, spectral identification comes from the Michigan Catalogue of Two dimensional spectral types (Houk and Cowley 1975¹⁶), which offers better spectral types identification than what is available from any studies in the the northern hemisphere.

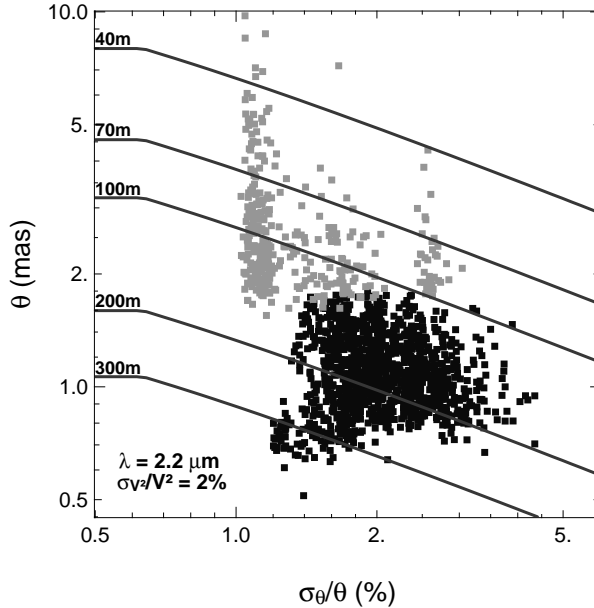


Figure 5. Comparison of cat. 1 (gray dots) and 2 (black dots) in the calibrator decision diagram. The 50, 100, 200 and 300 m curves plotted here, for the K band ($\lambda = 2.2 \mu m$), corresponds respectively to 35, 75, 145 and 220 m in the H band ($\lambda = 1.6 \mu m$) and 25, 55, 110 and 165 m in the J band ($\lambda = 1.2 \mu m$).

Band	σ_{V^2}/V^2		
	1 %	2 %	3 %
J	40 → 75 m	55 → 100 m	65 → 120 m
H	55 → 95 m	75 → 130 m	85 → 155 m
K	75 → 130 m	100 → 180 m	120 → 213 m

Table 2. Improvement of the median maximum baseline for J, H and K bands at the 1, 2 and 3 % visibility precision levels between cat. 1 and 2.

5.2. Baseline range

Fig. 5 shows a comparison between cat. 1 and 2 in the *calibrator decision diagram* (observations in the K band with a 2 % precision on the visibility), and illustrates the significant gain due to this work. Cat. 2 can be used to achieve a 2 % visibility error on the whole sky with baselines up to ~ 100 m, ~ 130 m, and ~ 180 m, in the J, H and K bands, respectively (see Table 2 for details). Therefore, our extended calibrator catalog fulfills the needs for calibration of the VLTI, the CHARA array, and any other 200-m class interferometers in the near infrared.

6. CONCLUSION

We have presented a list of 1630 stars selected to be used as calibrator stars for long baseline stellar interferometry. Among them, 374 come from the previous catalog compiled by Bordé et al. 2002.² The selection of the new stars was made according to the spectro-photometric criteria defined by,³ as well as additional ones that are specific to near-infrared interferometry. We used the work by³ to estimate the angular diameter from infrared photometric measurements extracted from IRAS and 2MASS catalogs. Our new catalog of interferometric calibrators is an homogeneous set of stars, provided with limb-darkened angular diameters and uniform disk angular diameters in J, H and K bands. Its intrinsic characteristics – a small list of stars with accurate angular diameters and uniform sky coverage – inherited from the previous version, were carefully maintained, while we included smaller stars in order to fulfill the needs of 200-m class interferometers, like the VLTI in the H band (and redder), and the CHARA array in the K band (and redder).

In this paper, we improved the performance of cat. 2 with respect to cat. 1 by extending the selection to fainter stars (this corresponds to going downwards on the calibrator decision diagram of Fig. 2). Now all eligible stars from the IRAS survey have been used in cat. 2, further extension is not possible in this direction. Improvements could still be obtained if/when more accurate photometry becomes available, which will result in smaller diameter errors (this corresponds to going leftwards on the calibrator decision diagram). For this, a dedicated observing program is needed as most of these sources are too bright for the major infrared surveys. From the decision diagram, it can be seen however that the gain to be expected is in a better sky coverage at 200–300 m baselines, rather than an extension of the maximum baseline for which cat. 2 would be useful. Another approach could be to use dwarf stars, see Kervella et al. in these proceedings: these stars are fairly close to us, allowing to discard easily binaries. Moreover, dwarfs seem to follow nicely Surface brightness/ photometric colors relations, allowing down to 1% precision on their diameter estimation.

7. ACKNOWLEDGEMENTS

This work has made use of the SIMBAD database, operated at CDS, Strasbourg, France. It also has made use of data products from the Two Micron All Sky Survey, which is a joint project of the University of Massachusetts and the Infrared Processing and Analysis Center/California Institute of Technology, funded by the National Aeronautics and Space Administration and the National Science Foundation. This work was performed in part under contract with the Jet Propulsion Laboratory (JPL) funded by NASA through the Michelson Fellowship Program. JPL is managed for NASA by the California Institute of Technology.

REFERENCES

1. G. Perrin, V. Coude Du Foresto, S. T. Ridgway, J.-M. Mariotti, W. A. Traub, N. P. Carleton, and M. G. Lacasse, “Extension of the effective temperature scale of giants to types later than M6,” *AAP* **331**, pp. 619–626, Mar. 1998.
2. P. Bordé, V. Coudé du Foresto, G. Chagnon, and G. Perrin, “A catalogue of calibrator stars for long baseline stellar interferometry,” *AAP* **393**, pp. 183–193, Oct. 2002.
3. J. G. Cohen, “The Spectra of Main-Sequence Stars in Galactic Globular Clusters. II. CH and CN Bands in M71,” *AJ* **117**, pp. 2434–2439, May 1999.
4. A. Richichi and I. Percheron, “CHARM: A Catalog of High Angular Resolution Measurements,” *AAP* **386**, pp. 492–503, May 2002.
5. J. Dommagnet and O. Nys, “The visual double stars observed by the Hipparcos satellite,” *AAP* **363**, pp. 991–994, Nov. 2000.
6. M. A. C. Perryman, L. Lindegren, J. Kovalevsky, E. Hoeg, U. Bastian, P. L. Bernacca, M. Crézé, F. Donati, M. Grenon, F. van Leeuwen, H. van der Marel, F. Mignard, C. A. Murray, R. S. Le Poole, H. Schrijver, C. Turon, F. Arenou, M. Froeschlé, and C. S. Petersen, “The HIPPARCOS Catalogue,” *AAP* **323**, pp. L49–L52, July 1997.
7. S. Malaroda, H. Levato, N. Morrell, B. García, M. Grosso, and G. J. Bolzicco, “Bibliographic catalogue of stellar radial velocities: (1991-1994),” *AAPS* **144**, pp. 1–4, May 2000.
8. J. R. de Medeiros and M. Mayor, “A catalog of rotational and radial velocities for evolved stars,” *AAPS* **139**, pp. 433–460, Nov. 1999.
9. D. L. Nidever, G. W. Marcy, R. P. Butler, D. A. Fischer, and S. S. Vogt, “Radial Velocities for 889 Late-Type Stars,” *APJS* **141**, pp. 503–522, Aug. 2002.
10. M. Cohen, W. A. Wheaton, and S. T. Megeath, “Spectral Irradiance Calibration in the Infrared. XIV. The Absolute Calibration of 2MASS,” *AJ* **126**, pp. 1090–1096, Aug. 2003.
11. J. A. Cardelli, G. C. Clayton, and J. S. Mathis, “The relationship between infrared, optical, and ultraviolet extinction,” *APJ* **345**, pp. 245–256, Oct. 1989.
12. M. Wittkowski, J. P. Aufdenberg, and P. Kervella, “Tests of stellar model atmospheres by optical interferometry. VLTI/VINCI limb-darkening measurements of the M4 giant ψ Phe,” *AAP* **413**, pp. 711–723, Jan. 2004.

13. A. Claret, "A new non-linear limb-darkening law for LTE stellar atmosphere models. Calculations for $-5.0 \leq \log[M/H] \leq +1$, $2000 \text{ K} \leq T_{eff} \leq 50000 \text{ K}$ at several surface gravities," *AAP* **363**, pp. 1081–1190, Nov. 2000.
14. G. Cayrel de Strobel, C. Soubiran, and N. Ralite, "Catalogue of $[Fe/H]$ determinations for FGK stars: 2001 edition," *AAP* **373**, pp. 159–163, July 2001.
15. M. S. Bessell, F. Castelli, and B. Plez, "Model atmospheres broad-band colors, bolometric corrections and temperature calibrations for O - M stars," *AAP* **333**, pp. 231–250, May 1998.
16. N. Houk and A. P. Cowley, *Michigan Catalogue of two-dimensional spectral types for the HD star*, Ann Arbor: University of Michigan, Departement of Astronomy, 1975, 1975.